Hindawi
Mathematical Problems in Engineering
Volume 2018, Article ID 1693184, 13 pages
https://doi.org/10.1155/2018/1693184

Research Article

Well Testing Model of Multiple Fractured Horizontal Well with Consideration of Stress-Sensitivity and Variable Conductivity in Tight Gas Reservoirs

Zhongwei Wu,[1] **Chuanzhi Cui**,[1] **Zhen Wang**,[1] **Yingfei Sui**,[1] **Peifeng Jia**,[1] **and Wenhao Tang**[2]

[1]*College of Petroleum Engineering, China University of Petroleum (East China), No. 66 Changjiang West Road, Qingdao 266580, Shangdong, China*
[2]*Hebei Scoilmic Petroleum Technology Co., Ltd, No. 40 Shuiyue Temple Main Street, Changzhou 061001, Hebei, China*

Correspondence should be addressed to Chuanzhi Cui; ccz2008@126.com

Received 23 May 2018; Accepted 5 August 2018; Published 6 September 2018

Academic Editor: Zhengbiao Peng

Multiple fractured horizontal wells have been widely used to develop unconventional tight gas reservoirs. Currently, many well testing models were established to study the performance of fractured horizontal wells in tight gas reservoirs. However, none of these models thoroughly takes stress-sensitivity of natural fractures and variable conductivity of artificial fractures into consideration. Based on the consideration of stress-sensitivity of natural fractures and variable conductivity of artificial fractures, a novel well testing model for fractured horizontal well in tight gas reservoirs is proposed. And the semianalytical solution of this new model is obtained by dividing the artificial fracture into different segments under the integrative methods of Laplace transformation, point source function, perturbation theory, superposition principle, and Stehfest numerical inversion. After validation, the semianalytical solution is consistent with that of Zerzar's model (2004). Also, typical pressure and pressure derivative curves are plotted. According to typical curves, seven regimes can be derived, namely, bilinear flow, linear flow, early-time pseudoradial flow, biradial flow, intermediate-time pseudoradial flow, and pseudo-steady state interporosity flow, and late-time pseudoradial flow can be identified. In addition, this paper analyzes the impact on pressure and pressure derivative curves exerted by variable conductivity and stress-sensibility. The results show that variable conductivity mainly affects the early flow regimes, including bilinear flow, linear flow, and early-time radial flow, while the stress-sensitivity mainly affects the later flow regimes, including intermediate-time pseudoradial flow, pseudo-steady state interporosity flow, and late-time pseudoradial flow. The typical curves will ascend with the increasing of stress-sensitivity coefficient. The research provides a method for precise prediction of formation parameters and has a significant impact on the tight gas reservoir development.

1. Introduction

The technology of multiple fractured horizontal well has become the mainstream method for exploiting tight gas reservoirs [1–4]. The pressure analysis of multiple fractured horizontal wells has a great significance to the development and optimization of tight gas reservoirs. In general, the natural fracture has developed in tight gas reservoirs [5, 6]. The natural fracture medium has the stress-sensitivity characteristic [5–9]. And along the extending direction, artificial fractures are mostly irregular [10, 11] and the proppant distribution is uneven [12], so the artificial hydraulic fracture is variable conductivity. Although there are many researches on pressure analysis of multiple fractured horizontal wells, they rarely take the stress-sensitivity of natural fractures and the variable conductivity of artificial fractures into consideration, simultaneously.

Zerzar et al. [13] researched the pressure characteristic of multiple hydraulically fractured horizontal wells. In Zerzar's work [13], the variable conductivity of fracture was neglected. Medeiros. et al. [14] discussed the performance of fractured horizontal well in a tight gas formation. In the work of Medeiros. et al. [14], hydraulic fracture was finite conductivity. The natural fractured zones around the hydraulic

fracture were double-porosity idealization. However, the stress-sensitivity of the tight gas reservoir was neglected and the conductivity of hydraulic fracture was a constant. Based on Green's functions and the source/sink method, Yao et al. [15] presented a semianalytical pressure analysis model of the multiple fractured horizontal well. In Yao's [15] work, the fracture was finite conductivity (the conductivity of fracture is a constant) and they did not consider the effect of stress-sensitivity in the tight gas reservoir on well performance. Guo et al. [16] established a coupling model for a multiple fractured horizontal well in tight reservoirs. During the establishment of the coupling model, finite conductivity of hydraulic fractures and stress-sensitivity of the reservoir were taken into account. However they did not take the effect of variable conductivity of hydraulic fracture on well performance into consideration. Xu et al. [17] established a coupling model of fractured horizontal well in tight oil reservoir by using Green functions and Newman product principle. In the study, the fracture was infinite conductivity and the stress-sensitivity was neglected. Chen et al. [18] proposed a semianalytical model for multiple fractured horizontal wells with consideration of pressure drop in wellbore. Although the finite conductivity of hydraulic fracture and stress-sensitivity of reservoir were taken into consideration, they treated tight gas reservoir as a single pore medium and the conductivity of hydraulic fracture was a constant. Zhang et al. [19] and Yin et al. [20] established a performance model of horizontal wells with multiple fractures in a tight oil reservoir. However, they did not take the stress-sensitivity and variable conductivity into consideration.

As stated above, many scholars have built the multiple fractured horizontal well testing model in tight gas/oil reservoirs, most of which assume the conductivity of the fractures to be infinite or constant. However, microseismic monitoring and experimental researches can observe complex fracture network during the fracturing process and along the extending direction of fractures which are mostly irregular such as wedge-shaped fractures [10].Therefore, fracture conductivity along the extending direction of fractures cannot be considered as a constant. This paper firstly establishes a multiple fractured horizontal well model with the consideration of variable fracture conductivity and stress-sensitivity of reservoir permeability in tight gas reservoirs. A novel semianalytical solution has been derived by utilizing Laplace transformation, point source function, perturbation theory, superposition principle, and Stehfest numerical inversion. The predictions by the proposed model are in good agreement with those of Zerzar's model [13]. According to the curves of dimensionless pressure and pressure derivative, seven flow regimes can be identified. Finally, the effects of relevant parameters are discussed, especially for the variable conductivity of artificial fractures.

2. Physical Model

Figure 1 shows the horizontal well with a series of vertical fractures. The fractures vertically intersect the y-axis, distribute at random along the y-axis, and extend along the x-axis. Figure 2 is the platform of a multifractured horizontal well in a laterally infinite reservoir. In order to establish this model, some assumptions are made as follows.

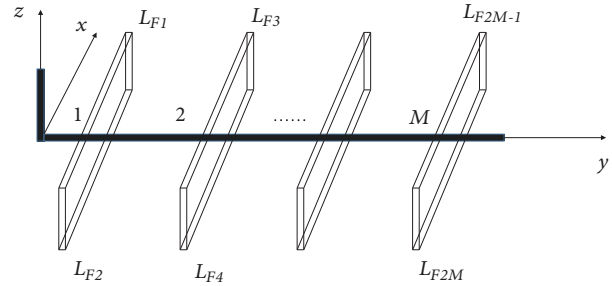

Figure 1: The illustration of multifractured horizontal well with variable conductivity fractures.

(1) Tight gas reservoirs are dual-porosity systems composed of matrix and natural fractures. Natural fracture system is stress-sensitivity. In other words, the permeability of natural fracture system varies with the effective stress. And the relationship between the permeability of natural fracture system and effective stress is a power exponential relation [21]. The height of the reservoir is constant with impermeable top and bottom boundaries.

(2) Two wings of each fracture may be of unequal length. The conductivity of each wing is different and even for the same fracture wing the conductivity is also a function of coordinates.

(3) Gas flow within natural fracture system can be described by Darcy's flow. Considering ultralow permeability of matrix, from matrix to fractures, the gas flow is pseudo-steady state interporosity flow.

(4) The multiple fractured horizontal well produces at a constant rate. However, the flow rate of each fracture is different.

(5) The initial pressure throughout the reservoir is uniform which equals p_i. The impacts of gravity and capillary force are neglected.

3. Mathematical Model

3.1. Dimensionless Definitions. For the sake of simplicity, the following dimensionless variables will be utilized.

The pseudopressure

$$m(p) = 2\int_{p_{sc}}^{p} \frac{p}{\mu z} dp \tag{1}$$

The dimensionless pseudopressure

$$m_D = \frac{\pi k_{fi} h T_{sc}}{P_{sc} Q_{sc} T} \left(m(p_i) - m(p)\right) \tag{2}$$

The dimensionless time

$$t_D = \frac{k_{fi} t}{\left(\phi_m C_{tm} + \phi_f C_{tf}\right) \mu_g \overline{L}_F^{\,2}} \tag{3}$$

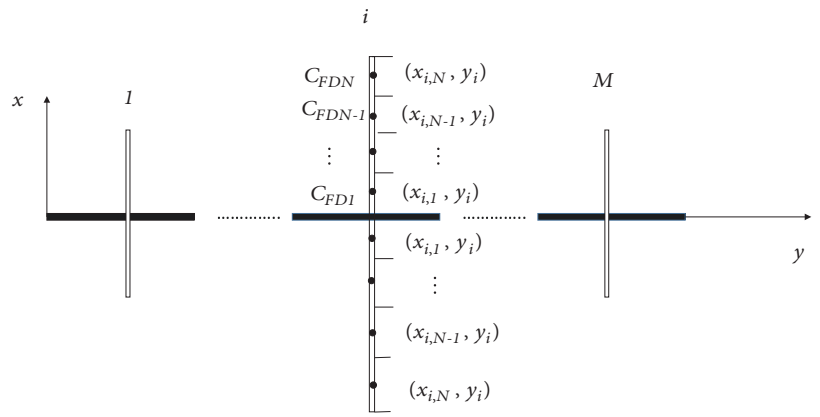

Figure 2: The schematic of discretion of a multiple fractured horizontal well.

The dimensionless cross flow coefficient

$$\lambda = \alpha \frac{k_m}{k_{fi}} \overline{L}_F^{\,2} \tag{4}$$

The dimensionless storability ratio

$$\omega_f = \frac{\phi_f C_{tf}}{\phi_m C_{tm} + \phi_f C_{tf}} \tag{5}$$

where L_F is the length of fracture wing, and the reference length is $\overline{L}_F$

$$\overline{L}_F = \frac{1}{2M} \sum_{j=1}^{2M} L_{Fi} \tag{6}$$

The dimensionless distance

$$\begin{aligned} y_D &= \frac{x}{\overline{L}_F}; \\ r_D &= \frac{x}{\overline{L}_F}; \\ x_D &= \frac{x}{L_F} \in [0, 1] \end{aligned} \tag{7}$$

The dimensionless flow rate

$$\begin{aligned} \widetilde{q}_{DF} &= \frac{\widetilde{q}_F}{Q_{sc}}; \\ \widetilde{q}_{DwF} &= \frac{\int_0^{L_F} \widetilde{q} dx}{Q_{sc}} \end{aligned} \tag{8}$$

The conductivity of each fracture wing, depending on the width and permeability of fractures, could be different. The dimensionless fracture wing conductivity can be defined as

$$C_{FD} = \frac{k_F w}{k_{fi} L_F} \tag{9}$$

The dimensionless stress-sensitivity coefficient

$$\gamma_D = \frac{\gamma p_{sc} Q_{sc} T}{\pi k_{fi} h T_{sc}} \tag{10}$$

3.2. Gas Reservoir Flow Model. The governing equations (the detailed derivation is given in Appendix A) can be obtained by integrating the respective continuity, motion, and state equations in the natural fracture and matrix systems. By applying the dimensionless variables defined above, the dimensionless form of the governing equations can be written as

Natural fracture system

$$\begin{aligned} &\frac{\partial^2 m_{Df}}{\partial {r_D}^2} + \frac{1}{r_D} \frac{\partial m_{Df}}{\partial r_D} + \gamma_D \left(\frac{\partial m_{Df}}{\partial r} \right)^2 \\ &\quad = e^{\gamma_D m_{Df}} \omega_f \frac{\partial m_{Df}}{\partial t_D} + e^{\gamma_D m_{Df}} \lambda \left(m_{Dm} - m_{Df} \right) \end{aligned} \tag{11}$$

Matrix system

$$-\lambda \left(m_{Dm} - m_{Df} \right) = \left(1 - \omega_f \right) \frac{\partial m_{Dm}}{\partial t_D} \tag{12}$$

The dimensionless form of initial condition

$$\begin{aligned} m_{Dm}\big|_{t_D \longrightarrow 0} &= 0; \\ m_{Df}\big|_{t_D \longrightarrow 0} &= 0 \end{aligned} \tag{13}$$

The dimensionless form of boundary condition

$$\begin{aligned} e^{-\gamma_D m_{Df}} r_D \left. \frac{\partial m_{Df}}{\partial r_D} \right|_{r_D \longrightarrow 0} &= -\widetilde{q}_D; \\ m_{Df}\big|_{r_D \longrightarrow \infty} &= 0 \end{aligned} \tag{14}$$

Petrobra's substitution is as follows:

$$m_D (r_D, t_D) = -\frac{1}{\gamma_D} \ln \left[1 - \gamma_D \zeta_D (r_D, t_D) \right] \tag{15}$$

According to the theory conducted by Wang [21], a parameter perturbation is performed in ζ_D by defining the following series:

$$\zeta_D = \zeta_{D0} + \gamma_D\zeta_{D1} + \gamma_D{}^2\zeta_{D2} + \gamma_D{}^3\zeta_{D3} + \gamma_D{}^4\zeta_{D4} + \cdots \quad (16a)$$

$$-\frac{1}{\gamma_D}\ln\left[1-\gamma_D\zeta_D\left(r_D,t_D\right)\right] = \zeta_D\left(r_D,t_D\right) + \frac{1}{2}\gamma_D\zeta_D{}^2\left(r_D,t_D\right) + \frac{1}{6}\gamma_D\zeta_D{}^3\left(r_D,t_D\right) + \frac{1}{24}\gamma_D\zeta_D{}^3\left(r_D,t_D\right) + \cdots \quad (16b)$$

$$\frac{1}{1-\gamma_D\zeta_D\left(r_D,t_D\right)} = 1 + \gamma_D\zeta_D\left(r_D,t_D\right) + \gamma_D{}^2\zeta_D\left(r_D,t_D\right) + \gamma_D{}^3\zeta_D\left(r_D,t_D\right) + \gamma_D{}^4\zeta_D\left(r_D,t_D\right) + \cdots \quad (16c)$$

By using (15), (16a), (16b), and (16c) to simplify (11)~(14), considering that the value of γ_D is very small, the zero-order perturbation solution can satisfy the accuracy requirement. Equations (11) ~ (14) can be rewritten as

$$\frac{\partial^2\zeta_{D0}}{\partial r_D{}^2} + \frac{1}{r_D}\frac{\partial\zeta_{D0}}{\partial r_D} = \omega_f\frac{\partial\zeta_{D0}\left(p_f\right)}{\partial t_D} - \lambda\left(m_D\left(p_m\right) - \zeta_{D0}\right) \quad (17)$$

$$-\lambda\left(m_{Dm} - \zeta_{D0}\right) = \left(1-\omega_f\right)\frac{\partial m_{Dm}}{\partial t_D} \quad (18)$$

$$m_{Dm}\big|_{t_D\longrightarrow 0} = 0; \qquad \zeta_{D0}\big|_{t_D\longrightarrow 0} = 0 \quad (19)$$

$$r_D\left.\frac{\partial\zeta_{D0}}{\partial r_D}\right|_{r_D\longrightarrow 0} = -\widetilde{q}_D; \qquad \zeta_{D0}\big|_{r_D\longrightarrow\infty} = 0 \quad (20)$$

Utilizing Laplace transformation, we can obtain (17)~(20) in Laplace domain

$$\frac{\partial^2\overline{\zeta}_{D0}}{\partial r_D{}^2} + \frac{1}{r_D}\frac{\partial\overline{\zeta}_{D0}}{\partial r_D} = f\left(s\right)\overline{\zeta}_{D0} \quad (21)$$

where $f(\mathrm{s}) = (s\omega_f(1-\omega_f)+\lambda)/(s(1-\omega_f)+\lambda)$

$$r_D\left.\frac{\partial\overline{\zeta}_{D0}}{\partial r_D}\right|_{r_D\longrightarrow 0} = -\overline{\widetilde{q}}_D; \qquad \overline{\zeta}_{D0}\big|_{r_D\longrightarrow\infty} = 0 \quad (22)$$

$$\overline{\zeta}_{D0}\big|_{t_D\longrightarrow 0} = 0 \quad (23)$$

The instantaneous point source solution can be obtained with integration of (21)~(23) [22]. On the basis of the mirror reflected method and superposition principle, the continuous point solution in Laplace domain in infinite gas reservoirs with impermeable top and bottom boundaries can be derived as

$$\overline{\zeta}_{D0} = \overline{\widetilde{q}}_D K_0\left(r_D\sqrt{sf\left(s\right)}\right) \quad (24)$$

Then, the pressure response of i-th segment at (x, y) is

$$\overline{\zeta}_{D0} = \frac{\overline{q}_{Di}}{\Delta x_{Di}} \cdot \int_{-\Delta x_{Di}/2}^{\Delta x_{Di}/2} K_0\left(\sqrt{sf\left(s\right)}\sqrt{\left(x_D - x_{Di} - u\right)^2 + \left(y_D - y_{Di}\right)^2}\right)du \quad (25)$$

Based on the superposition principle, the pressure response at (x_{Di}, y_{Di}),$(1 \le j \le N*2M)$ caused by $N*2M$ segments can be obtained as follows:

$$\overline{\zeta}_{D0}\left(x_{Dj}, y_{Dj}\right) = \sum_{j=1}^{N*2M}\overline{\zeta}_{Dm0}\left(x_{Dm}, y_{Dm}\right) \quad (26)$$

Substituting (25) into (26), (26) can be rewritten in the matrix form

$$\mathbf{B}\times\mathbf{q_D} = \boldsymbol{\zeta}_{\mathbf{D0}} \quad (27)$$

where

$$\mathbf{B} = \begin{bmatrix} B_{1.1} & \cdots & B_{1.k} & \cdots & B_{1.N*2M} \\ \cdots & \cdots & \cdots & \cdots & \cdots \\ B_{k.1} & \cdots & B_{k.k} & \cdots & B_{k.N*2M} \\ \cdots & \cdots & \cdots & \cdots & \cdots \\ B_{N*2M.1} & \cdots & B_{N*2M.k} & \cdots & B_{N*2M.N*2M} \end{bmatrix} \quad (28)$$

$$B_{i.j} = \frac{1}{\Delta x_{Di}} \cdot \int_{-\Delta x_{Di}/2}^{\Delta x_{Di}/2} K_0\left(\sqrt{sf\left(s\right)}\sqrt{\left(x_{Dj} - x_{Di} - u\right)^2 + \left(y_{Dj} - y_{Di}\right)^2}\right)du \quad (29)$$

$$\boldsymbol{\zeta}_{\mathbf{D0}} = \left[\overline{\zeta}_{D0,1}\ \ \overline{\zeta}_{D0,2}\ \ \cdots\ \ \overline{\zeta}_{D,N*2M}\right]^{\mathrm{T}} \quad (30)$$

$$\mathbf{q_D} = \left[\overline{q}_{D1}\ \ \overline{q}_{D2}\ \ \cdots\ \ \overline{q}_{DN*2M}\right]^{\mathrm{T}} \quad (31)$$

3.3. Fracture Flow Model. The gas flow differential equation in artificial fracture system is as follows:

$$\frac{\partial}{\partial x}\left(\frac{k_F wh}{\mu}\frac{\partial p_F}{\partial x}\right) + \widetilde{q}_F\left(\mathrm{x}\right) = \phi_F C_{tF}\frac{\partial p_F}{\partial t} \quad (32)$$

Since the compressibility of C_{tF} is very small and can be negligible, then, (32) can be written as

$$\frac{\partial}{\partial x}\left(\frac{k_F wh}{\mu}\frac{\partial p_F}{\partial x}\right) + \widetilde{q}_F\left(\mathrm{x}\right) = 0 \quad (33)$$

The inner boundary condition

$$\frac{k_F wh}{\mu}\left.\frac{\partial p_F}{\partial x}\right|_{x=0} = q_{wF} \quad (34)$$

The outer boundary condition

$$\left.\frac{\partial p_F}{\partial x}\right|_{x=L_F} = 0 \tag{35}$$

The initial condition

$$p_F(x, t=0) = p_i \tag{36}$$

Dividing the j-th fracture wing into N equal parts and taking the Laplace transformation of ((16a), (16b), (16c))~(18), the pressure response of the i-th segment can be expressed as follows (the detailed derivation is given in Appendix B):

$$\begin{aligned}\overline{m}_{DF}(x_{Di}) = \overline{m}_{wDN} &+ \pi\Delta x_D \sum_{j=1}^{i-2}\left[\overline{q}_{DF}(x_{Dj})\sum_{n=j+1}^{i}\frac{1}{C_{FDn}}\right] \\ &+ \pi\Delta x_D \frac{\overline{q}_{DF}(x_{Di-1})}{C_{FDi}}\frac{2\pi}{s} \\ &- \sum_{j=1}^{i-1} x_{Dj}\left(\frac{1}{C_{FDj}} - \frac{1}{C_{FDj+1}}\right) - \frac{2\pi x_{Di}}{sC_{FDi}}\end{aligned} \tag{37}$$

Equation (37) can be written in the matrix form

$$\mathbf{m_{wDN}} - \mathbf{C} \times \mathbf{q_{DF}} = \mathbf{m_{DF}} \tag{38}$$

$$\mathbf{q_{DF}} = \left[\overline{q}_{DF1}\ \ \overline{q}_{DF2}\ \ \cdots\ \ \overline{q}_{DFN*2M}\right]^{\mathrm{T}} \tag{39}$$

$$\mathbf{m_{wDN}} = \left[\overline{m}_{wDN}\ \ \overline{m}_{wDN}\ \ \cdots\ \ \overline{m}_{wDN}\right]^{\mathrm{T}} \tag{40}$$

3.4. Semianalytical Solution. According to the continuity of the pressure and flux along the fracture surface in the process of seepage, we can obtain the following equations:

$$\begin{aligned}\overline{m}_{DF}(x_D, y_D) &= \overline{\zeta}_{D0}(x_D, y_D); \\ \overline{q}_{DF}(x_D, y_D) &= \overline{q}_D(x_D, y_D)\end{aligned} \tag{41}$$

The total flow rate is the summation of the flow from each fracture:

$$\sum_{j=1}^{N*2M} s\overline{q}_{Dj} = 1 \tag{42}$$

Combining (27)~(31) and (38)~(42), we can obtain

$$\begin{bmatrix} & & -1 \\ \mathbf{C}+\mathbf{B} & \cdots & \\ & & -1 \\ s & \cdots\ s & 0 \end{bmatrix} \times \begin{bmatrix} \mathbf{q_{DF}} \\ \overline{m}_{wDN} \end{bmatrix} = \mathbf{b} \tag{43}$$

$$\mathbf{b} = \left[0\ \ 0\ \ \cdots\ \ 0\ \ 1\right]^{\mathrm{T}} \tag{44}$$

By solving (43), we can obtain the wellbore pressure and the flux distribution in the artificial fracture in Laplace domain, which can be further inverted to the real time space with Stehfest numerical algorithm [23]. According to (15), the solution with consideration of stress-sensitivity of natural fracture system can be obtained

$$m_{wD}(r_D, t_D) = -\frac{1}{\gamma_D}\ln\left[1 - \gamma_D m_{wDN}(r_D, t_D)\right] \tag{45}$$

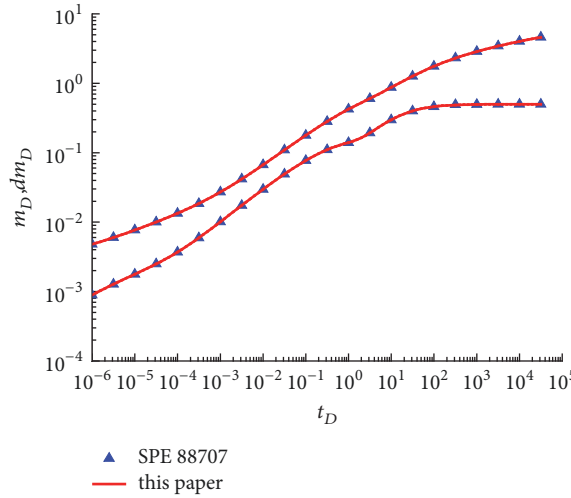

Figure 3: Comparison of dimensionless pressure and pressure derivative for a horizontal well intercepted by 3 finite-conductivity fractures ($C_{FD} = 20$, $FS = 10$) with the solution presented by Aissa Zerzar [13], SPE 88707.

4. Model Validation

To validate our results, the data of a horizontal well intercepted by three vertical fractures in the literature [13] is selected. The conductivity of hydraulic fracture is a constant ($C_{FD} = 20$). The curves of dimensionless pressure and pressure derivative presented in this paper are compared with the work of Aissa et al. in Figure 3. As can be seen from Figure 3, the results obtained in this paper show excellent agreement with those of Aissa Zerzar's model.

5. Results and Discussion

In order to more authentically reflect the actual characteristics of fractures, a multiple fractured horizontal well model is proposed in this paper with the simultaneous consideration of various influences, such as unequal length and different conductivity fractures, nonuniform distribution of fractures along the horizontal well, and variable conductivity within each wing along the extending direction of fractures (the conductivity of each part of fracture can be different). However, for the convenience of studying the impact of variable conductivity in the fracture extending direction on the pressure response of fractured horizontal well, parameters are selected to plot the corresponding curves with the assumption that all the wings of fractures have the same properties and consist of two different conductivities.

5.1. Flow Characteristics Analysis. In this section, the dimensionless pressure and pressure derivative curves for fractured

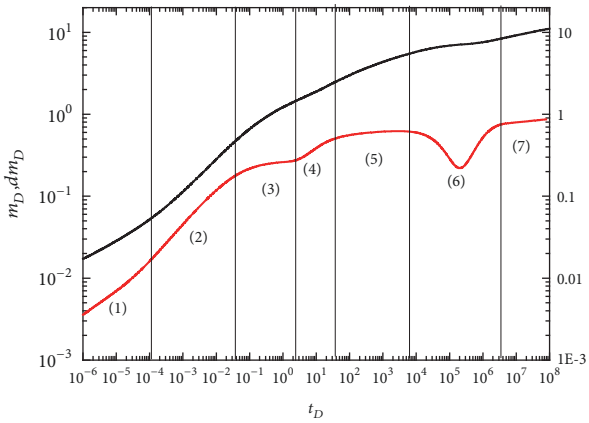

FIGURE 4: The curves of dimensionless pressure and pressure derivative.

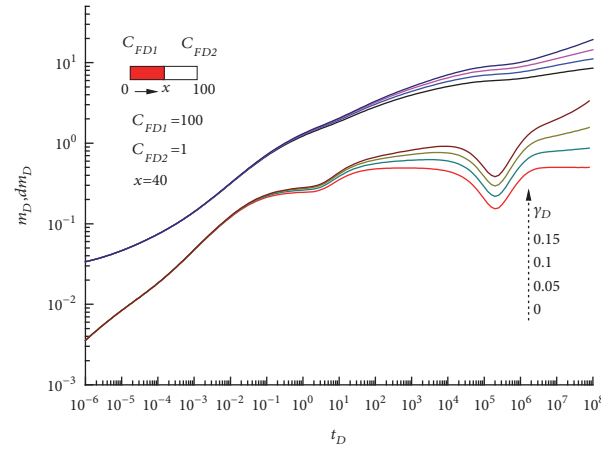

FIGURE 5: The curve of pressure and pressure derivative with different dimensionless stress-sensitivity coefficient.

horizontal well are computed with the proposed well testing model and the effects of relevant parameters are analyzed.

Figure 4 shows the typical well testing curves for fractured horizontal well. The values of relevant parameters in Figure 4 are listed as follows. The values of relevant parameters in Figure 4 are listed as follows: $\overline{L}_F = 100m$; $N = 5$; $M = 2$; $\omega_f = 0.1$; $FS = 20$; $\lambda = 10^{-6}$; $C_{FD1} = 10$; $C_{FD2} = 500$; and $\gamma_D = 0.05$. It can be seen from Figure 4 that there are seven flow regimes for a multiple fractured horizontal well in tight gas reservoirs.

(1) Bilinear flow period: during this stage, both the dimensionless pressure and pressure derivative curves have a straight line with a slope of 1/4. Gas flows from the reservoirs to artificial fractures and from artificial fractures to wellbore simultaneously. This region only occurs when the fracture conductivity is finite.

(2) Early-time linear flow: both pressure and pressure derivative curves are characterized by a slope of 1/2 straight line. During this period, gas flows linearly from formation to individual fractures and each fracture produces independently, and the interference between different fractures has not occurred yet.

(3) Early-time radial flow: during this period, the value of the pressure derivative curve is "1/2M" where M is the number of fractures. Early radial flow time depends on the half length of fracture and distance between fractures.

(4) Biradial flow period: during this period, the pressure and pressure derivative curves are two parallel lines. Pressure waves reach the adjacent fractures, and the interference between different fractures gradually becomes apparent.

(5) Intermediate pseudoradial flow: during this period, the pressure derivative curve is characterized by a horizontal line with a value of 0.5. The interporosity flow coefficient determines the occurrence time of this stage.

(6) Pseudo-steady state interporosity flow, which is marked by a "dip" in the pressure derivative curve: the interporosity flow coefficient represents fluid ability from matrix to fracture system. The dimensionless storability ratio mainly affects the "dip" shape on pressure derivative type curves.

(7) Late-time pseudoradial flow period: without stress-sensitivity, the pressure derivative curve is a horizontal line with a value of 0.5. However, when considering the effect of the stress-sensitivity, the pressure derivative curve is no longer a horizontal line but bends upward, which indicates the faster pressure drop.

5.2. Effect of Stress-Sensitivity on Type Curves. Figure 5 shows the impact of dimensionless stress-sensitivity coefficient on pressure and pressure derivative curves of fractured horizontal wells in tight gas reservoirs. The values of relevant parameters are listed as follows: $\overline{L}_F = 100m$; $N = 5$; $M = 2$; $\omega_f = 0.1$; $FS = 20$; $\lambda = 10^{-6}$; $C_{FD1} = 10$; $C_{FD2} = 500$; $\gamma_D = 0.05, 0.08, 0.1$; $x = 40m$. Figure 5 reveals that the dimensionless stress-sensitivity factor mainly affects the late flow regimes, including early-time pseudoradial flow, pseudo-steady state interporosity flow, and late-time radial flow. The greater the dimensionless stress-sensitivity coefficient is, the higher the pressure and pressure derivative curves in the late flow stages bend upwards. According to the microscopic mechanism of tight gas reservoirs, the natural fractures gradually close with the decrease of formation pressure. As a result, natural fracture permeability decreases and the flow resistance increases. Therefore, formation pressure drops faster in order to maintain a constant production, which manifests upward on pressure and pressure derivative curves.

5.3. Effect of Variable Fracture Conductivity. For the sake of studying the impact of variable conductivity in the fracture extending direction on the pressure response of fractured horizontal well, the influence of stress-sensitivity has to be reduced; thus a small enough value of dimensionless stress-sensitivity coefficient is set to be 0.01. The values of other relevant parameters are listed as follows: $\overline{L}_F = 100m$; $N = 5$; $M = 2$; $\omega_f = 0.1$; $FS = 20$; $\lambda = 10^{-6}$; $C_{FD1} = 10$; $C_{FD2} = 500$. The pressure and pressure derivative curves are, respectively, shown in Figures 6 and 7. These two figures are the pressure and pressure derivative curves of fractured horizontal wells considering variable fracture conductivity,

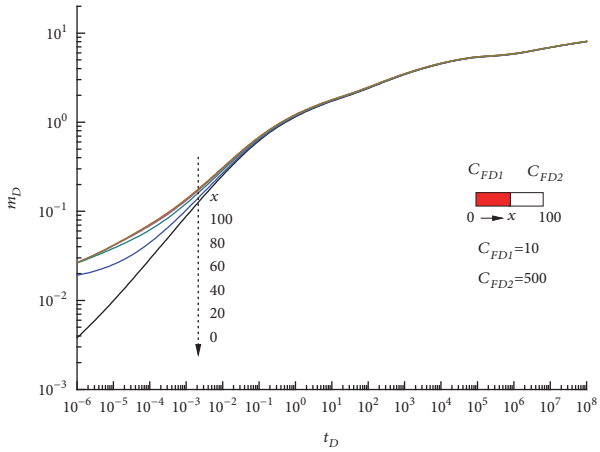

FIGURE 6: The curves of pressure with varied length of low conductivity nearby the well.

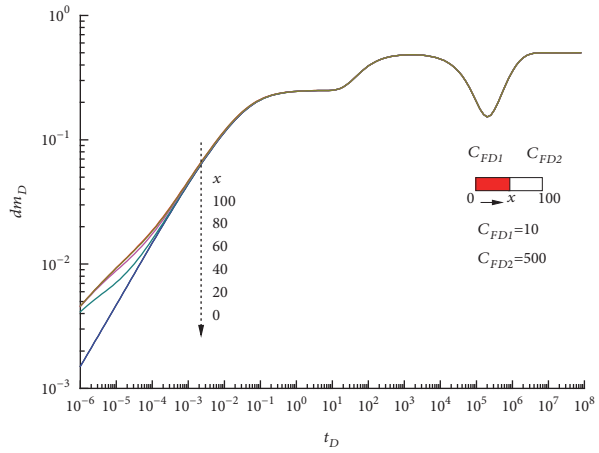

FIGURE 7: The curves of pressure derivative with varied length of low conductivity nearby the well.

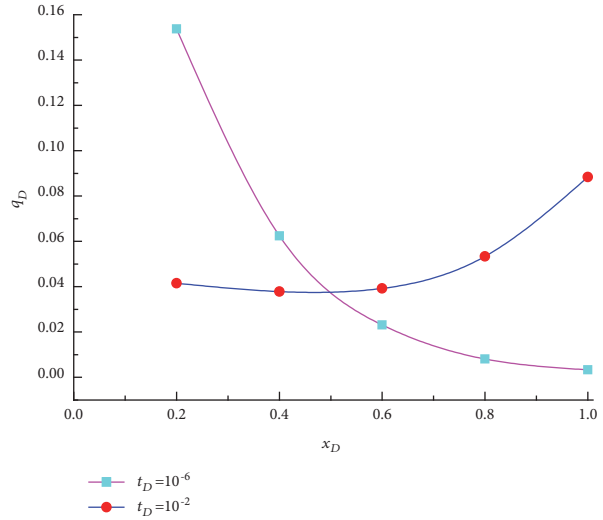

FIGURE 8: The curves of flow distribution in the fracture at different times.

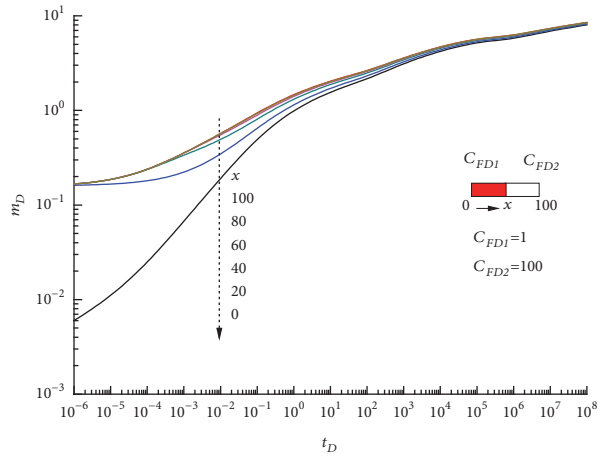

FIGURE 9: The curves of pressure with varied length of low conductivity nearby the well.

respectively. Variable fracture conductivity nearby the wellbore is low while in the fracture extreme it is high. From Figures 6 and 7, we can see that the pressure and pressure derivative curves considering variable conductivity are closer to those of $x = 0$ ($C_{FD} = 10$) at the beginning of bilinear flow period. It indicates that the low fracture conductivity dominates the flow in this case. However, as time increases, the curves gradually approach the pressure and pressure derivative curves of $x = 100$ ($C_{FD} = 500$), indicating that the flow is gradually controlled by the high conductivity section of fractures. It can also be observed from Figures 6 and 7 that the appearance of flow controlled by the high conductivity part of fractures will be delayed with the increase of x.

In order to better explain the phenomenon above, the flux distributions of gas flow from the formation to fractures at $t_D = 10^{-6}$ and $t_D = 10^{-2}$ are plotted (shown in Figure 8). Figure 8 shows that most gas enters from the part of fractures near the wellbore. Due to the low fracture conductivity near the wellbore, the resistance of gas flow from formation to fractures is large. Meanwhile, the low conductivity section near the wellbore greatly increases the resistance of gas flow from fractures into the horizontal wellbore. Therefore, the flow at the initial period is mainly affected by the low conductivity part of fractures. Figure 8 illustrates that the main part of gas flow from the formation into fractures occurs in the extreme of fracture at $t_D = 10^{-2}$. Thanks to the higher conductivity of the extreme of fractures, the flow at this time is controlled by the higher conductivity. As x increases, the proportion of high-conductivity fractures decreases and the appearance of flow controlled by high-conductivity fractures will be delayed.

Figures 9 and 10 show the pressure and pressure derivative curves with the values of $C_{FD1} = 1$ and $C_{FD2} = 100$, respectively, while other parameters are the same with Figures 6 and 7. It can be seen that Figures 9 and 6 (or Figures 10 and 7) have similar results. The lower conductivity near the wellbore contributes to the more apparent transition performance on curves from low conductivity to high conductivity. But the

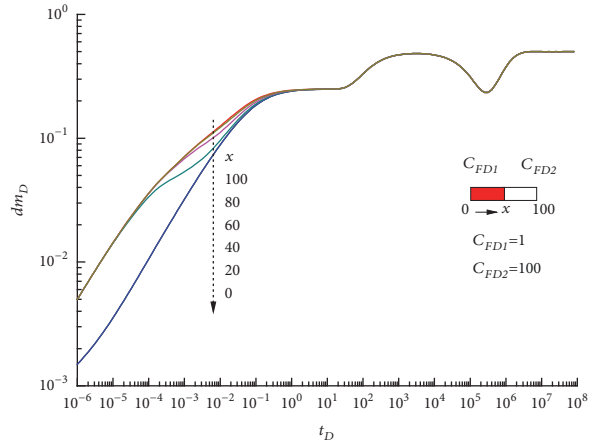

FIGURE 10: The curves of pressure derivative with varied length of low conductivity nearby the well.

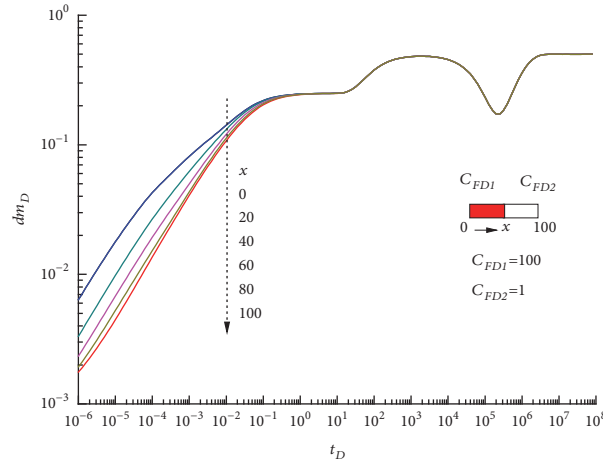

FIGURE 12: The curves of pressure derivative with varied length of high conductivity nearby the well.

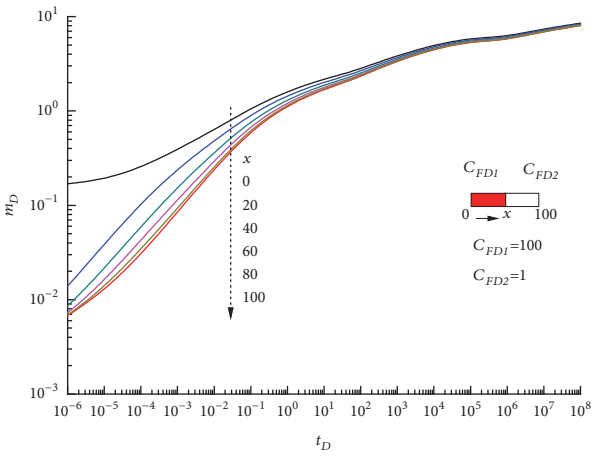

FIGURE 11: The curves of pressure with varied length of high conductivity nearby the well.

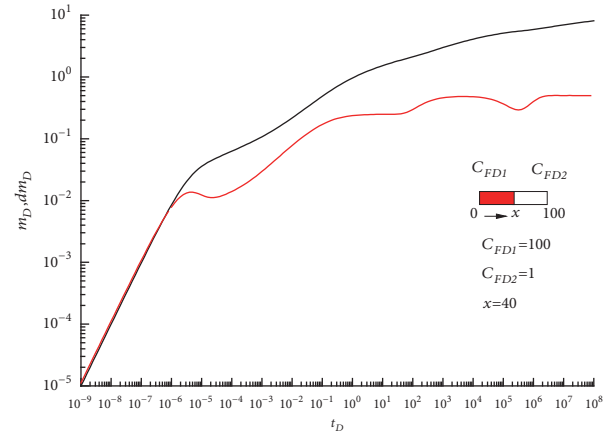

FIGURE 13: The curves of pressure and pressure derivative with the consideration of wellbore storage and skin factor.

initial time of early radial flow is approximately the same, free from the impact of the variable conductivity.

A set of parameters are given to calculate the pressure and pressure derivative curves shown in Figures 11 and 12 (conductivity nearby the wellbore is high while in the fracture extreme it is is low). The values of these parameters are listed as follows: $\overline{L}_F = 100m$; $N = 5$; $M = 2$; $\omega_f = 0.1$; $FS = 20$; $\lambda = 10^{-6}$; $C_{FD1} = 100$; $C_{FD2} = 1$; $\gamma_D = 0.01$. Figures 11 and 12 show that, as x increases, the pressure and pressure derivative curves gradually switch from the pressure and pressure derivative curves for $x = 0$ ($C_{FD} = 1$) to $x = 100$ ($C_{FD} = 100$). The main reasons are the same as in Figures 6 and 7. Figure 12 also shows that the pressure derivative curve considering variable fracture conductivity is closer to the curve for $x = 100$. It is the main reason that the portion of fractures near the wellbore is not only the major part where gas flows from formation into fractures at the beginning of flow, but also the path where gas flows from other portions of fractures into the horizontal wellbore. Consequently, the portion of fractures near the wellbore has greater impact on variable conductivity curves. With the increase of x, the total conductivity of variable conductivity fractures increases and the early radial flow appears in advance.

5.4. Effect of Wellbore Storage and Skin. Applying Duhamel's principle, the dimensionless bottom-hole pressure derived in Laplace space incorporating wellbore storage coefficient and skin factor can be expressed as follows:

$$\overline{m}_{wD} = \frac{s\overline{m}_{wDN} + S}{s + C_D s^2 \left(s\overline{m}_{wDN} + S\right)} \tag{46}$$

The values of relevant parameters are listed as follows: $\overline{L}_F = 100m$; $N = 5$; $M = 2$; $\omega_f = 0.1$; $FS = 20$; $\lambda = 10^{-6}$; $C_{FD1} = 100$; $C_{FD2} = 1$; $\gamma_D = 0.01$; $x = 40m$; $S = 0.1$; $C_D = 10^{-3}$. It can be observed in Figure 13 that both pressure and pressure derivative curves are marked by a 1 slope straight line which is influenced by wellbore storage. The pressure derivative curve shows a "hump" when the flow regime is affected by skin factor and the pressure.

6. Conclusions

(1) A well testing model of multiple fractured horizontal well with consideration of stress-sensitivity of natural fractures and variable conductivity of artificial fractures in tight gas reservoirs is proposed. The results of the proposed model in this paper show good agreement with those of Zerzar's model.

(2) There are seven flow regimes for multiple fractured horizontal well in tight gas reservoirs, in time order, which are bilinear flow, linear flow, early-time pseudoradial flow, biradial flow, intermediate-time pseudoradial flow, pseudo-steady state interporosity flow, and late-time pseudoradial flow.

(3) The variable conductivity affects the typical curves in the early flow regimes, including bilinear flow, linear flow, and early-time pseudoradial flow. And the stress-sensitivity of natural fractures affects the typical curves in the late flow regimes, including intermediate-time pseudoradial flow, pseudo-steady state interporosity flow, and late-time radial flow. The typical curves will ascend with the increasing of stress-sensitivity coefficient.

Appendix

A.

Here we briefly describe the derivation of partial differential equation for matrix and natural fracture systems. For radial coordinate, the continuity equation in natural fracture system can be expressed as

$$\frac{1}{r}\frac{\partial\left(r\rho_f v_f\right)}{\partial r} = \frac{\partial\left(\rho_f\phi_f\right)}{\partial t} + q_m \tag{A.1}$$

Assuming that the interporosity flow from the matrix to the fractures is in a pseudo-steady state, the interporosity flow equation neglecting the percolation flow in the matrix can be written as

$$q_m = -\alpha\rho\frac{k_m}{\mu}\left(p_m - p_f\right) \tag{A.2}$$

The continuity equation in matrix system can be expressed as

$$q_m = \frac{\partial\left(\rho_m\phi_m\right)}{\partial t} \tag{A.3}$$

Gas state equation, gas compressibility factor, and formation compressibility factor can be expressed, respectively, as

$$\rho = \frac{pM}{ZRT} \tag{A.4}$$

$$C_{gl} = \frac{1}{\rho_l}\frac{\partial\rho_l}{\partial p_l};$$

$$C_{\phi l} = \frac{1}{\phi_l}\frac{\partial\phi_l}{\partial p_l} \tag{A.5}$$

$$\left(l = m, f\right)$$

Combining (A.1)~(A.5), the following equations can be obtained:

$$\frac{1}{r}\frac{\partial}{\partial r}\left(r\frac{p_f}{\mu Z}\frac{\partial p_f}{\partial r}\right) = \frac{p_f\phi_f C_{tf}}{Zk_f}\frac{\partial p_f}{\partial t} - \frac{1}{2}\alpha\frac{k_m}{k_f}\left(\frac{p_m^2}{\mu Z} - \frac{p_f^2}{\mu Z}\right) \tag{A.6}$$

$$-\frac{1}{2}\alpha k_m\left(\frac{{p_m}^2}{\mu Z} - \frac{{p_f}^2}{\mu Z}\right) = \frac{\phi_m C_{tm} p_m}{Z}\frac{\partial p_m}{\partial t} \tag{A.7}$$

Substituting pseudopressure equation into (A.6) and (A.7), the following equations can be obtained:

$$\frac{\partial^2 m\left(p_f\right)}{\partial r^2} + \frac{1}{r}\frac{\partial m\left(p_f\right)}{\partial r} = \frac{\mu\phi_f C_{tf}}{k_f}\frac{\partial m\left(p_f\right)}{\partial t} - \alpha\frac{k_m}{k_f}\left[m\left(p_m\right) - m\left(p_f\right)\right] \tag{A.8}$$

$$-\alpha\frac{k_m}{k_f}\left[m\left(p_m\right) - m\left(p_f\right)\right] = \frac{\mu\phi_m C_{tm}}{k_f}\frac{\partial m\left(p_m\right)}{\partial t} \tag{A.9}$$

Based on the stress-sensitivity equation [21], the relationship between pseudopressure and permeability is defined as

$$k_f = k_{fi}e^{-\gamma\left(\mathrm{m}_i - \mathrm{m}_f\right)} \tag{A.10}$$

Substituting (A.9) and (A.10) into (A.8), we can get the governing equation

$$\frac{\partial^2 m\left(p_f\right)}{\partial r^2} + \frac{1}{r}\frac{\partial m\left(p_f\right)}{\partial r} + \gamma\left(\frac{\partial m\left(p_f\right)}{\partial r}\right)^2 = e^{\gamma\left[m_i - m\left(p_f\right)\right]}\frac{\mu\phi_f C_{tf}}{k_f}\frac{\partial m\left(p_f\right)}{\partial t} + \lambda\left[m\left(p_m\right) - m\left(p_f\right)\right] \tag{A.11}$$

B.

Here we briefly describe the derivation of the solution of flow model in artificial fracture system. With the definitions of the dimensionless variables, the dimensionless equations such as the governing equation, inner boundary condition, outer boundary condition, and initial condition can be expressed as follows.

The dimensionless transient seepage flow equation in artificial fracture system

$$\frac{\partial}{\partial x_D}\left(C_{FD}\frac{\partial m_{DF}}{\partial x_D}\right) = 2\pi\tilde{q}_{DF}\left(\mathrm{x}_D\right) \tag{B.1}$$

The dimensionless inner boundary condition

$$\left.\frac{\partial m_{DF}}{\partial x_D}\right|_{x_D=0} = -\left(\frac{2\pi q_{Dw F}}{C_{FD}}\right)_{x_D=0} \tag{B.2}$$

The dimensionless outer boundary condition

$$\left.\frac{\partial m_{DF}}{\partial x_D}\right|_{x_D=1} = 0 \tag{B.3}$$

The dimensionless initial condition

$$m_{DF}\left(x_D, t_D = 0\right) = 0, \quad 0 < x_D < 1 \tag{B.4}$$

With the Laplace transformation, we can obtain the following equations:

$$\frac{\partial}{\partial x_D}\left(C_{FD}\frac{\partial \overline{m}_{DF}}{\partial x_D}\right) = 2\pi L_F \overline{\overline{q}}_{DF}\left(\mathrm{x}_D\right) \tag{B.5}$$

$$\left.\frac{\partial \overline{m}_{DF}}{\partial x_D}\right|_{x_D=0} = -\left(\frac{2\pi \overline{q}_{DwF}}{C_{FD}}\right)_{x_D=0} \tag{B.6}$$

$$\left.\frac{\partial \overline{m}_{DF}}{\partial x_D}\right|_{x_D=1} = 0 \tag{B.7}$$

$$\overline{m}_{DF}\left(x_D, 0\right) = 0 \tag{B.8}$$

Integrating for 0 to x_D, (B.5) can be rewritten as

$$\begin{aligned}&\int_0^{x_D} \frac{\partial}{\partial x_D}\left(C_{FD}\frac{\partial \overline{m}_{DF}}{\partial x_D}\right) dx_D \\ &\quad = \int_0^{x_D} 2\pi L_F \overline{\overline{q}}_{DF}\left(x_D\right) dx_D\end{aligned} \tag{B.9}$$

Then

$$\begin{aligned}&C_{FD}\left.\frac{\partial \overline{m}_{DF}}{\partial x_D}\right|_{u=x_D} - C_{FD}\left.\frac{\partial \overline{m}_{DF}}{\partial x_D}\right|_{u=0} \\ &\quad = \int_0^{x_D} 2\pi L_F \overline{\overline{q}}_{DF}\left(x_D\right) dx_D\end{aligned} \tag{B.10}$$

Substituting (B.6) into (B.10), we can obtain

$$C_{FD}\frac{\partial \overline{m}_{DF}}{\partial x_D} + 2\pi \overline{q}_{DwF} = \int_0^{x_D} 2\pi L_F \overline{\overline{q}}_{DF}\left(x_D\right) dx_D \tag{B.11}$$

Integrating both sides of (B.11) from 0 to x_D

$$\begin{aligned}&\int_0^{x_D} C_{FD}\frac{\partial \overline{m}_{DF}}{\partial x_D} dx_D + \int_0^{x_D} 2\pi \overline{q}_{DwF} dx_D \\ &\quad = \int_0^{x_D}\int_0^{x_D} 2\pi L_F \overline{\overline{q}}_{DF}\left(x_D\right) dx_D dx_D\end{aligned} \tag{B.12}$$

Equation (B.12) can be simplified as

$$\begin{aligned}&\int_0^{x_D} C_{FD}\partial \overline{m}_{DF} + 2\pi x_D \overline{q}_{DwF} \\ &\quad = 2\pi L_F x_D \int_0^{x_D} \overline{\overline{q}}_{DF}\left(x_D\right) dx_D \\ &\quad - 2\pi L_F \int_0^{x_D} x_D \overline{\overline{q}}_{DF}\left(x_D\right) dx_D\end{aligned} \tag{B.13}$$

We divide each wing of a fracture into N equal segments and assume each discrete segment can be seen as a surface source with a uniform flux density, so the pressure response of the i-th segment can be obtained

$$\begin{aligned}&\sum_{j=1}^{i} C_{FDj}\int_{x_{Dj-1/2}}^{x_{Dj+1/2}} \partial \overline{m}_{DF} + 2\pi x_{Di}\overline{q}_{DwF} \\ &\quad = 2\pi L_F x_{Di}\sum_{j=1}^{i} \overline{\overline{q}}_{DF}\left(x_{Dj}\right)\int_{x_{Dj-1/2}}^{x_{Dj+1/2}} dx_D \\ &\quad - 2\pi L_F \sum_{j=1}^{i} \overline{\overline{q}}_{DF}\left(x_{Dj}\right)\int_{x_{Dj-1/2}}^{x_{Dj+1/2}} x_{Dj} dx_D\end{aligned} \tag{B.14}$$

Define

$$\begin{aligned}\Delta x_D &= x_{i+1/2} - x_{i-1/2}; \\ x_{i+1/2} &= x_i + \frac{\Delta x_D}{2}; \\ x_{i-1/2} &= x_i - \frac{\Delta x_D}{2}\end{aligned} \tag{B.15}$$

where $\Delta x = L_F/N$; $\Delta x_D = 1/N$
Substituting (B.15) into (B.14), we have

$$\begin{aligned}&\sum_{j=1}^{i} C_{FDj}\left(\overline{m}_{DF}\left(x_{Dj+1/2}\right) - \overline{m}_{DF}\left(x_{Dj-1/2}\right)\right) \\ &\quad + 2\pi x_{Di}\overline{q}_{DwF} \\ &\quad = 2\pi L_F x_{Di}\Delta x_D \sum_{j=1}^{i} \overline{\overline{q}}_{DF}\left(x_{Dj}\right) \\ &\quad - 2\pi L_F \Delta x_D \sum_{j=1}^{i} x_{Dj}\overline{\overline{q}}_{DF}\left(x_{Dj}\right)\end{aligned} \tag{B.16}$$

For $i = 1$, (B.16) becomes

$$\begin{aligned}&C_{FD1}\left(\overline{m}_{DF}\left(x_{D1}\right) - \overline{m}_{DF}\left(x_{D0}\right)\right) + 2\pi x_{D1}\overline{q}_{DwF} \\ &\quad = 2\pi L_F x_{D1}\Delta x_D \overline{\overline{q}}_{DF}\left(x_{D1}\right) \\ &\quad - 2\pi L_F \Delta x_D \sum_{m=1}^{i} \overline{\overline{q}}_{DF}\left(x_{D1}\right)\end{aligned} \tag{B.17}$$

Since $\overline{m}_{DF}(x_{D0}) = \overline{m}_{wDN}$, (B.17) can be simplified as follows:

$$\overline{m}_{DF}\left(x_{D1}\right) = \overline{m}_{wDN} - \frac{2\pi x_{D1}\overline{q}_{DwF}}{C_{FD1}} \tag{B.18}$$

For $i = 2$

$$\begin{aligned} & C_{FD1}\left(\overline{m}_{DF}\left(x_{D1}\right)-\overline{m}_{DF}\left(x_{D0}\right)\right) \\ & \quad + C_{FD2}\left(\overline{m}_{DF}\left(x_{D2}\right)-\overline{m}_{DF}\left(x_{D1}\right)\right) \\ & \quad + 2\pi x_{D2}\overline{q}_{DwF} \\ & = 2\pi L_F x_{D2}\Delta x_D\left(\overline{\tilde{q}}_{DF}\left(x_{D1}\right)+\overline{\tilde{q}}_{DF}\left(x_{D2}\right)\right) \\ & \quad - 2\pi L_F\Delta x_D\left(x_{D2}\overline{\tilde{q}}_{DF}\left(x_{D2}\right)+x_{D1}\overline{\tilde{q}}_{DF}\left(x_{D1}\right)\right) \end{aligned} \tag{B.19}$$

Substituting (B.18) into (B.19) yields

$$\begin{aligned} \overline{m}_{DF}\left(x_{D3}\right) = \overline{m}_{wDN} & + 2\pi L_F{\Delta x_D}^2\frac{\overline{\tilde{q}}_{DF}\left(x_{D1}\right)}{C_{FD2}} \\ & - 2\pi L_F x_{D1}\overline{q}_{DwF}\left(\frac{1}{C_{FD1}}-\frac{1}{C_{FD2}}\right) \\ & - \frac{2\pi x_{D2}\overline{q}_{DwF}}{C_{FD2}} \end{aligned} \tag{B.20}$$

For $i = 3$

$$\begin{aligned} & C_{FD1}\left(\overline{m}_{DF}\left(x_{D1}\right)-\overline{m}_{DF}\left(x_{D0}\right)\right)+C_{FD2}\left(\overline{m}_{DF}\left(x_{D2}\right)\right. \\ & \quad \left.-\overline{m}_{DF}\left(x_{D1}\right)\right)+C_{FD3}\left(\overline{m}_{DF}\left(x_{D3}\right)\ -\overline{m}_{DF}\left(x_{D2}\right)\right) \\ & \quad + 2\pi x_{D3}\overline{q}_{DwF} = 2\pi L_F x_{D3}\Delta x_D\left(\overline{\tilde{q}}_{DF}\left(x_{D1}\right)\right. \\ & \quad \left.+\overline{\tilde{q}}_{DF}\left(x_{D2}\right)+\overline{\tilde{q}}_{DF}\left(x_{D3}\right)\right) \\ & \quad - 2\pi L_F\Delta x_D\left(x_{D3}\overline{\tilde{q}}_{DF}\left(x_{D3}\right)+x_{D2}\overline{\tilde{q}}_{DF}\left(x_{D2}\right)\right. \\ & \quad \left.+x_{D1}\overline{\tilde{q}}_{DF}\left(x_{D1}\right)\right) \end{aligned} \tag{B.21}$$

Substituting (B.18) and (B.20) into (B.21) yields

$$\begin{aligned} & \overline{m}_{DF}\left(x_{D3}\right) \\ & \quad = \overline{m}_{wDN} - 2\pi x_{D1}\overline{q}_{DwF}\left(\frac{1}{C_{FD1}}-\frac{1}{C_{FD2}}\right) \\ & \qquad - 2\pi x_{D2}\overline{q}_{DwF}\left(\frac{1}{C_{FD2}}-\frac{1}{C_{FD3}}\right) \\ & \qquad - \frac{2\pi x_{D3}\overline{q}_{DwF}}{C_{FD3}} \\ & \qquad + 2\pi L_F{\Delta x_D}^2\overline{\tilde{q}}_{DF}\left(x_{D1}\right)\left(\frac{1}{C_{FD2}}+\frac{1}{C_{FD3}}\right) \\ & \qquad + 2\pi L_F{\Delta x_D}^2\frac{\overline{\tilde{q}}_{DF}\left(x_{D2}\right)}{C_{FD3}} \end{aligned} \tag{B.22}$$

From the derivation above, the pressure response of the i-th segment of fracture can be obtained as follows:

$$\begin{aligned} & \overline{m}_{DF}\left(x_{Di}\right) \\ & \quad = \overline{m}_{wDN} \\ & \qquad + 2\pi L_F{\Delta x_D}^2\sum_{j=1}^{i-2}\left[\overline{\tilde{q}}_{DF}\left(x_{Dj}\right)\sum_{n=j+1}^{i}\frac{1}{C_{FDn}}\right] \\ & \qquad + 2\pi L_F{\Delta x_D}^2\frac{\overline{\tilde{q}}_{DF}\left(x_{Di-1}\right)}{C_{FDi}} \\ & \qquad - 2\pi\overline{q}_{DwF}\sum_{j=1}^{i-1}x_{Dm}\left(\frac{1}{C_{FDj}}-\frac{1}{C_{FDj+1}}\right) \\ & \qquad - \frac{2\pi x_{Di}\overline{q}_{DwF}}{C_{FDi}} \end{aligned} \tag{B.23}$$

Assuming that the flux distribution of each discrete segment was uniform, then

$$\begin{aligned} \overline{q}_{DF}\left(x_{Di-1}\right) & = \Delta x_D L_F\overline{\tilde{q}}_{DF} = \Delta x\overline{\tilde{q}}_{DF}\left(x_{Di-1}\right) \\ & = \overline{q}_{DF}\left(x_{Di-1}\right) \end{aligned} \tag{B.24}$$

$$\overline{q}_{DwF} = \sum_{j=1}^{N}\overline{q}_{DF}\left(x_{Dm}\right) \tag{B.25}$$

Combining (B.23), (B.24), and (B.25), the following equation can be obtained:

$$\begin{aligned} & \overline{m}_{DF}\left(x_{Di}\right) \\ & \quad = \overline{m}_{wDN} \\ & \qquad + 2\pi L_F\Delta x_D\sum_{j=1}^{i-2}\left[\overline{q}_{DF}\left(x_{Dj}\right)\sum_{n=j+1}^{i}\frac{1}{C_{FDn}}\right] \\ & \qquad + 2\pi L_F\Delta x_D\frac{\overline{q}_{DF}\left(x_{Di-1}\right)}{C_{FDi}} \\ & \qquad - 2\pi\overline{q}_{DwF}\sum_{j=1}^{i-1}x_{Dj}\left(\frac{1}{C_{FDj}}-\frac{1}{C_{FDj+1}}\right) \\ & \qquad - \frac{2\pi x_{Di}\overline{q}_{DwF}}{C_{FDi}} \end{aligned} \tag{B.26}$$

Nomenclature

C_{FD}: Dimensionless fracture conductivity
S: Skin factor, dimensionless
t_D: Dimensionless time
C_D: Dimensionless wellbore storage factor
m: Pseudopressure, Pa/s
m_D: Dimensionless pseudopressure
m_{Dm}: Dimensionless matrix system pseudopressure
m_{Df}: Dimensionless natural fracture system pseudopressure
m_{DF}: Dimensionless artificial fracture system pseudopressure
s: Laplace variable
$\overline{m}_{wDN}$: Dimensionless bottom pressure ignoring skin factor and the wellbore storage in Laplace domain
$\overline{m}_{wD}$: Dimensionless bottom pressure considering skin factor and the wellbore storage in Laplace domain
$\overline{m}_D$: Dimensionless pseudopressure in Laplace domain
$\overline{m}_{Df}$: Dimensionless pseudopressure of natural fracture system in Laplace domain
$\overline{m}_{DF}$: Dimensionless pseudopressure of artificial fracture system in Laplace domain
$K_0(x)$: Modified Bessel function of second kind, zero order
ρ: Gas density kg/m^3
ρ_{sc}: Gas density at standard condition, kg/m^3
$\tilde{q}$: Surface flow rate of the line sink, m^3/s
$\overline{\tilde{q}}$: $\tilde{q}$ in Laplace domain
$\tilde{q}_D$: Dimensionless $\tilde{q}$, $m^3/s \cdot m$
$\overline{\tilde{q}}_D$: Dimensionless $\tilde{q}$ in Laplace domain
$\tilde{q}_F$: Flow rate per unit fracture length, $m^3/s \cdot m$
$\tilde{q}_{DF}$: Dimensionless flow rate per unit fracture length, m^3/s
$\overline{\tilde{q}}_{DF}$: Dimensionless flow rate per unit fracture length in Laplace domain
$\overline{q}_{DFi}$: Dimensionless flow rate of the i-th element in Laplace domain
q_{wF}: The total flow rate of one fracture wing, m^3/s
q_{DwF}: Dimensionless total flow rate of one fracture wing
$\overline{q}_{DwF}$: Dimensionless total flow rate of one fracture wing in Laplace domain
M: Number of fractures
N: Discrete number of each fracture wing
p_{sc}: Standard pressure, Pa
p_m: Matrix pressure, Pa
p_f: Pressure of natural fracture system, Pa
p_F: Pressure of artificial fracture system, Pa
p_i: Initial formation pressure, Pa
T_{sc}: Standard temperature, K
T: Reservoir temperature, K
h: Formation thickness, m
k_m: Matrix permeability, m^2
k_f: Natural fracture system permeability, m^2
k_{fi}: Natural fracture system permeability at initial condition, m^2
k_F: Artificial fracture system permeability, m^2
FS: Distance between fractures, m
L_F: The length of fracture wing, m
$\overline{L}_F$: The average length of fracture wings, m
Q_{sc}: Constant surface production rate of the horizontal well, m^3/s
w: Fracture width, m
ϕ_l: Porosity
λ: Interporosity flow coefficient, dimensionless
ω_f: Storativity ratio, dimensionless
C_{tl}: Compressibility, Pa^{-1}
μ: Viscosity, $Pa \cdot s$
Z: Gas deviation factor
$x.y$: x,y coordinates, m
Δx_{Di}: Dimensionless length of the i-th fracture element on the x coordinate
r: Radial distance, $r = \sqrt{x^2 + y^2}, m$
r_D: Dimensionless radial distance, $r_D = \sqrt{x_D{}^2 + y_D{}^2}$
ΔL_F: Distance between artificial fractures, m
t: Time, s
γ_D: Dimensionless stress-sensitivity coefficient
γ: Stress-sensitivity coefficient, Pa^{-1}

Subscripts

f: Natural fracture system
D: Dimensionless
m: Matrix system
F: Artificial fracture system
i: Initial condition
sc: Standard state.

Data Availability

The data used to support the findings of this study are included within the article.

Conflicts of Interest

The authors declare that they have no conflicts of interest.

Acknowledgments

This work is supported by the Fundamental Research Funds for the Central Universities through grant number 18CX06011A, China University of Petroleum Graduate Innovation Engineering Project through grant number YCX2018013, National Massive Oil & Gas Field and Coalbed Methane Development Program through grant number 2016ZX05010-002-007, National Science and Technology Major Demonstration Project "Tight Oil Development Demonstration Project of Bohai Bay Basin Jiyang Depression" through grant number 2016ZX05072006-004, and Shandong Provincial Natural Science Foundation through grant number ZR2017MEE054.

References

[1] S. Q. Peng and W. C. Zhao, "The adaptability study for developing tight gas reservoirs using horizontal wells," *Applied Mechanics and Materials*, vol. 423-426, pp. 614–617, 2013.

[2] T. Guo, S. Zhang, H. Ge, X. Wang, X. Lei, and B. Xiao, "A new method for evaluation of fracture network formation capacity of rock," *Fuel*, vol. 140, pp. 778–787, 2015.

[3] T. Guo, S. Zhang, Y. Zou, and B. Xiao, "Numerical simulation of hydraulic fracture propagation in shale gas reservoir," *Journal of Natural Gas Science and Engineering*, vol. 26, pp. 847–856, 2015.

[4] J. Zeng, X. Wang, J. Guo, F. Zeng, and Q. Zhang, "Composite linear flow model for multi-fractured horizontal wells in tight sand reservoirs with the threshold pressure gradient," *Journal of Petroleum Science and Engineering*, vol. 165, pp. 890–912, 2018.

[5] R. Zhang, L. Zhang, R. Wang, Y. Zhao, and R. Huang, "Simulation of a multistage fractured horizontal well in water-bearing tight fractured gas reservoir considering non-darcy flow," *Journal of Geophysics & Engineering*, vol. 15, pp. 877–894, 2018.

[6] S. Yin, D. Lv, and W. Ding, "New method for assessing microfracture stress sensitivity in tight sandstone reservoirs based on acoustic experiments," *International Journal of Geomechanics*, vol. 18, Article ID 04018008, 2018.

[7] J. Ji, Y. Yao, S. Huang, X. Ma, S. Zhang, and F. Zhang, "Analytical model for production performance analysis of multi-fractured horizontal well in tight oil reservoirs," *Journal of Petroleum Science and Engineering*, vol. 158, pp. 380–397, 2017.

[8] Z. Yang, H. Yang, H. Chen, and H. Zhang, "Method for Evaluating Rock Stress Sensitivity for Low-Permeability Tight Gas Reservoirs," *Chemistry Technology of Fuels & Oils*, vol. 53, pp. 68–76, 2017.

[9] X. P. Li, L. N. Cao, C. Luo, B. Zhang, J. Q. Zhang, and X. H. Tan, "Characteristics of transient production rate performance of horizontal well in fractured tight gas reservoirs with stress-sensitivity effect," *Journal of Petroleum Science & Engineering*, vol. 158, pp. 92–106, 2017.

[10] J. Guo, Q. Lu, and F. Zeng, "A productivity prediction model for a fractured well with wedge-shaped fractures," *Shiyou Xuebao/Acta Petrolei Sinica*, vol. 34, no. 2, pp. 346–352, 2013.

[11] T. Guo, Y. Li, Y. Ding, Z. Qu, N. Gai, and Z. Rui, "Evaluation of Acid Fracturing Treatments in Shale Formation," *ENERGY & FUELS*, vol. 31, no. 10, pp. 10479–10489, 2017.

[12] M. Roostaei, A. Nouri, V. Fattahpour, and D. Chan, "Numerical simulation of proppant transport in hydraulic fractures," *Journal of Petroleum Science and Engineering*, vol. 163, pp. 119–138, 2018.

[13] A. Zerzar, D. Tiab, and Y. Bettam, "Interpretation of multiple hydraulically fractured horizontal wells," in *Proceedings of the 11th ADIPEC: Abu Dhabi International Petroleum Exhibition and Conference*, pp. 455–467, UAE, October 2004.

[14] F. Medeiros Jr., E. Ozkan, and H. Kazemi, "Productivity and drainage area of fractured horizontal wells in tight gas reservoirs," *SPE Reservoir Evaluation & Engineering*, vol. 11, no. 5, pp. 902–911, 2008.

[15] S. Yao, F. Zeng, H. Liu, and G. Zhao, "A semi-analytical model for multi-stage fractured horizontal wells," *Journal of Hydrology*, vol. 507, pp. 201–212, 2013.

[16] J. Guo, H. Wang, and L. Zhang, "Transient pressure behavior for a horizontal well with multiple finite-conductivity fractures in tight reservoirs," *Journal of Geophysics and Engineering*, vol. 12, no. 4, pp. 638–656, 2015.

[17] M.-Y. Xu, Q.-Q. Ran, G.-Z. Shen, and N. Li, "A study on unsteady seepage field of fractured horizontal well in tight gas reservoir," *Journal of the Energy Institute*, vol. 88, no. 1, pp. 87–92, 2015.

[18] Z. Chen, X. Liao, X. Zhao, L. Zhu, and H. Liu, "Performance of multiple fractured horizontal wells with consideration of pressure drop within wellbore," *Journal of Petroleum Science and Engineering*, vol. 146, pp. 677–693, 2016.

[19] F. Zhang and D. T. Yang, "Effects of Non-Darcy Flow and Penetrating Ratio on Performance of Horizontal Wells with Multiple Fractures," *Journal of Energy Resources Technology*, vol. 140, no. 3, pp. 1–11, 2018.

[20] F. Yin, Q. Y. Li, P. C. Li, Y. Guo, Y. R. An, and D. T. Lu, "GPU-Based Computation of Formation Pressure for Multi-stage Hydraulically Fractured Horizontal Wells in Tight Oil and Gas Reservoirs," *Mathematical Problems in Engineering*, pp. 1–11, 2018.

[21] H.-T. Wang, "Performance of multiple fractured horizontal wells in shale gas reservoirs with consideration of multiple mechanisms," *Journal of Hydrology*, vol. 510, pp. 299–312, 2014.

[22] E. Ozkan and R. Raghavan, "New solutions for well-test-analysis problems. Part 1. Analytical considerations," *SPE Formation Evaluation*, vol. 6, no. 3, pp. 359–368, 1991.

[23] H. Stehfest, "Numerical inversion of Laplace transforms," *Communications of the ACM*, vol. 13, no. 1, pp. 47–49, 1970.